

Fluorescence Intermittency Limits Brightness in CdSe/ZnS Nanoparticles Quantified by Fluorescence Correlation Spectroscopy

Jennifer A. Rochira,^{†,‡} Manasa V. Gudheti,[‡] Travis J. Gould,[‡] Ryan R. Laughlin,[‡] Jay L. Nadeau,^{§,||} and Samuel T. Hess^{*,‡}

Functional Genomics Interdisciplinary Ph.D. Program, University of Maine, Orono, Maine 04469, Department of Physics and Astronomy and Institute for Molecular Biophysics, University of Maine, Orono, Maine 04469, Department of Biomedical Engineering, McGill University, Montréal, Québec, Canada, and Institute for Molecular Biophysics, The Jackson Laboratory, Bar Harbor, Maine 04609

Received: October 30, 2006; In Final Form: November 9, 2006

Traditional fluorophores often impose inconvenient limitations because of their narrow excitation spectra, broad emission bands, and significant photobleaching. Quantum dots (QDs) have grown in popularity because of their high emission quantum yields, broad absorbance spectra, and narrow, tunable emission spectra. Here, coated CdSe/ZnS QDs with emission maxima at 496 nm (T2–496), ~520 nm (QD520), and ~560 nm (QD560 and Qdot565) were characterized while freely diffusing in solution using confocal fluorescence correlation spectroscopy (FCS) and were compared with well-known fluorophores such as Alexa 488 to reveal critical photophysical properties. Comparisons are made between dots synthesized by similar methods (QD520 and QD560 nm) differing in their emission spectra and outer coating for biofunctionalization. The same photophysical principles also describe the T2–496 and Qdot565 dots, which were synthesized by different, proprietary methods. All of the tested QDs had larger hydrodynamic radii and slower diffusion coefficients than Alexa 488 and underwent numerous transitions between bright and dark states, especially at high illumination intensities, as described here by a new FCS fitting function. The QDs with the fastest transitions between the bright and dark states had the lowest average occupancies in dark states and correspondingly higher maximum brightness per particle. Although these QDs were in some cases brighter than Alexa at low excitation intensities, the QDs saturated at lower intensities than did Alexa and had generally somewhat lower maximum brightness per particle, except for the Qdot565s. Thus, it appears that intermittency (at least in part) limits maximum brightness in QDs, despite the potential for high fluorescence emission rates that is expected from their large extinction coefficients. These results suggest possibilities for significant improvement of QDs for biological applications by adjustments of manufacturing techniques and environmental conditions.

Introduction

Because of their advantageous properties, semiconductor quantum dots (QDs) have attracted a great deal of interest for biological imaging applications. Their narrow,¹ tunable emission spectra^{2–5} and broad absorption spectra^{1,6} permit imaging a large number of different probes simultaneously;^{3,7} their large extinction coefficients^{8,9} and two-photon excitation cross sections¹⁰ require less excitation laser power, thus minimizing photooxidation and photodamage of intracellular contents and permitting excitation of probes located deep inside blood or scattering tissue.^{9,10}

A wide variety of biological applications are now possible as a result of novel bioconjugated nanoparticles. QDs with surface-attached antibodies¹¹ are used routinely to label plasma membrane proteins,¹² for long-term imaging of multiple species in living cells,⁷ and for ultrasensitive (single dot) detection.¹¹ Numerous successful biological applications detailed else-

where^{9,13,14} also include multiphoton microscopy,¹⁰ QD-peptides, which targeted probe particles to tumor vasculature,¹⁵ QD-nucleotide conjugates,¹⁶ and protein-QD conjugates,^{4,11} used to stain mammalian cell lines¹¹ and visualize receptor-mediated endocytosis.²

Because of their resistance to photobleaching^{11,17} and their high brightness^{11,12,18} compared to organic dyes excited under the same conditions, more photons can be collected from a QD than from an organic fluorophore, a key quantity in single particle imaging applications.

Fluorescence intermittency,¹⁹ also called blinking (typically on 10^{-2} – 10^1 s timescales) and flicker (here defined as occurring on timescales $<10^{-2}$ s), provides a complication to understanding the photophysics of these particles. Often involving large numbers of states with a power-law distribution of off-times,²⁰ QD intermittency often results from interconversions between states of different fluorescence brightness and spans a broad range of timescales.²⁰

The significantly enhanced extinction coefficients of many QDs (compared with organic fluorophores) are expected to result in greater excitation rates of QDs at the same excitation laser power and also should result in a higher rate of emission per molecule (i.e., higher molecular brightness).⁹ However, the frequently observed intermittency of QDs^{19,21,22} reduces fluo-

* Corresponding author. E-mail: sam.hess@umit.maine.edu. Tel.: 207-581-1036. Fax: 207-581-3410.

[†] Functional Genomics Interdisciplinary Ph.D. Program, University of Maine.

[‡] Department of Physics and Astronomy and Institute for Molecular Biophysics, University of Maine.

[§] McGill University.

^{||} The Jackson Laboratory.

rescence brightness, as fewer particles are in emitting states at any given time. In fact, under some conditions intermittency can cause the maximum molecular brightness to be less than that of some of the best organic fluorophores. Furthermore, flicker and blinking on timescales of experimental interest can be highly undesirable (unless well understood), especially if they are dependent on environmental parameters such as ion or dissolved gas concentrations, excitation power, and illumination wavelength, as these parameters are often variables in biological imaging experiments.

While single molecule techniques are ideally suited to the determination of flicker and blinking properties of these probes,^{23,24} further quantitative information is needed to reveal the key characteristics that optimize QD brightness and resistance to photobleaching, while reducing blinking and flicker. For example, how do the brightness per particle and intermittency of freely diffusing QDs depend on core size, coating, and synthesis method? How does the number of states involved in flicker depend on excitation intensity? Better understanding of these important variables will lead to improved probe characteristics for the specific needs of biological imaging: maximal collected photons within a narrow time window or over repeated excitations in long series of image acquisitions.

We report the results of a comparative study of QD photo-physics using fluorescence correlation spectroscopy (FCS) to determine key properties of relevance to biological imaging applications. Count rate per molecule, fluorescence intermittency, and extinction coefficient are determined for QDs of varying core size and synthesis method. A new analytical FCS fitting function is introduced that successfully describes the autocorrelation of all QDs tested over 3 orders of magnitude in excitation intensity. Finally, as QD probes are increasingly being used to label intracellular compartments, we determined diffusion coefficients and hydrodynamic radii of the same QDs and tested QD behavior in the presence of physiologically relevant ion concentrations. It is our hope that this information can be used to successfully optimize the use of QDs in living biological systems.

Methods

FCS. For FCS measurements, the 488 nm or 514 nm lines from an argon-ion laser (Omnichrome, Melles Griot, Carlsbad, CA) or diode-pumped solid-state laser at 405 nm (BCL-405-15, low noise model, CrystaLaser, Reno, NV) were steered by turning mirrors and a periscope assembly into the back port of an inverted microscope (IX71, Olympus America, Melville, NY). Powers from the resonators were controlled with a combination of two optical density filters. After passing through appropriate interference cleanup filters (488 nm: Z488/10, Chroma, Brattleboro, VT. 514 nm: Z514/10, Chroma, Brattleboro, VT), the laser beam then was reflected by a dichroic mirror (see filter sets below) and was focused by an Olympus 1.2 NA/60× water immersion objective onto the sample, held in an 8-well sample chamber with ~0.5 mL/well and borosilicate 0.17 mm coverslip bottom (Labtek II; Nalge-Nunc, Rochester, NY). Fluorescence was collected through the same objective, passing through the dichroic mirror and emission filters before being focused by the 180 mm tube lens into an optical fiber with 50 μm core diameter, mounted on an *x-y-z* translation stage. Filter sets used and measured transmission wavelength ranges were blue, 440–545 nm; green, 508–563 nm; and orange, 547–627 nm.

The fluorescence was carried by the fiber to the detector, a fiber-coupled avalanche photodiode, or APD (EG & G Perkin-

Elmer model SPCM-AQR-14-FC, Pacer Components, Berkshire, U.K.). The APD signal was processed using either of two correlator cards (Flex2K-100 and Flex99-100; Correlator.com, Bridgewater, NJ), and the average fluorescence intensity (0.1 s integration time) and autocorrelation were recorded. Integration time for the autocorrelation (1–300 s) and number of runs (20–300) were adjusted depending on signal-to-noise ratio and frequency of large (bright) objects in the observation volume. Origin (Microcal Software, Inc.) software was used to fit and characterize the autocorrelation. All components except the laser power supply, computer, and monitor were mounted on a vibration-isolated air table.

Correlation curves were initially fitted using the following standard function from literature:²⁵

$$G_x(\tau) = \frac{1}{N} \frac{1}{(1 + \tau/\tau_D)} \frac{1}{(1 + \tau/\omega^2\tau_D)^{0.5}} \prod_{i=1}^m \frac{1 - F_i + F_i e^{-k_i\tau}}{1 - F_i} \quad (1)$$

where N denotes the mean number of fluorescent molecules diffusing in the excitation volume. Diffusion kinetics in the Gaussian intensity profile (with lateral-to-axial-dimension ratio ω) are characterized by the diffusion time (τ_D). The exponential decay terms describe the dynamics of m independent transitions between states of different spectroscopic properties (e.g., states of different fluorescence brightness under the given experimental conditions), which include photoconversion, chemical kinetics, and transitions between singlet and triplet states.¹⁴ The fraction F_i of molecules residing in a dark state for duration τ_i can be determined from the measurements, where $m = 0$ or $F_i = 0$ for diffusion alone.

The excitation rate (k_x), which is equal to the number of times per second a molecule in the focal volume will be excited (on average), at a given excitation wavelength (λ_x) is equal to

$$k_x = \sigma I \quad (2)$$

where σ is the excitation cross section calculated from the extinction coefficient using $\sigma = (3.82 \times 10^{-21} \text{ cm}^3 \text{ M})(\epsilon)$, and I is the excitation intensity. The quantum yield for photoconversion (flicker) is calculated using $\phi = dk_f/dk_x$, where k_f is the flicker rate, such as that obtained from fitting $G(\tau)$ using eq 1.

Calibration of FCS Setup. The well-characterized fluorophores Alexa 488 and Alexa 546 (A-20000 and A-20002; Molecular Probes, Eugene, OR), and Rhodamine B (Sigma-Aldrich, St. Louis, MO) were used as calibration standards for the concentration and diffusion coefficient of the QDs. Alexa was diluted 500-fold with high-pressure liquid chromatography (HPLC) water for a 500 μL total volume and placed in a 1 cm cuvette. Absorbance was measured at 494 nm using a DU Series 7000 diode array spectrophotometer (Beckman Instruments, Inc.) and was used to determine the stock concentration by Beer's Law, $C = A/\epsilon L$, where A is absorbance, L is the absorbance path length (typically either 1 cm in a standard cuvette or an effective path length of 1 mm or 0.1 mm in the nanodropper), and ϵ is the extinction coefficient as specified from literature. The extinction coefficient of Alexa 488 was taken from Molecular Probes ($\epsilon_{\text{Alexa}} = 73\,000 \pm 500 \text{ M}^{-1} \text{ cm}^{-1}$ at 494 nm). This corresponds to an original stock concentration of $1.452 \pm 0.017 \text{ mM}$. For Alexa 488, Alexa 546, and Rhodamine B, a typical concentration for FCS was ~10 nM that was subsequently diluted 10-fold at higher intensities at which the count rate would have exceeded the maximum allowable by the detector.

Using FCS, the number of molecules (N) of Alexa in the observable volume was determined from the autocorrelation curve, where $G(0) = 1/N$. The concentration of an unknown C_{unk} (i.e., the concentration of QDs) was determined using the known concentration of Alexa (C_{calib}) by

$$C_{\text{unk}} = C_{\text{calib}} \frac{N_{\text{unk}}}{N_{\text{calib}}} \quad (3)$$

where N_{unk} and N_{calib} are the background-corrected total number of molecules in the unknown and Alexa samples, respectively.

Sample Preparation. Samples of T2-496 (Evident Type II EviTags with Lake Placid Blue ~496 nm nominal emission, solubilized in water) were used as received from Evident Technologies or diluted in HPLC water to concentrations ~10 nM for FCS. The original stock solution had a nominal concentration of 15 μM in water (given by the manufacturer). Original stocks of Qdot 565 amino (PEG) QDs (originally in 50 mM borate buffer, pH 8.3) were diluted to ~1 nM solutions with high purity liquid chromatography (HPLC) grade water, excited at 514 nm and detected from 547 to 627 nm using the orange filter combination (see above).

Synthesis of QD520s and QD560s. CdSe/ZnS “core-shell” nanocrystals were synthesized as described previously.²⁶ In brief, CdSe/ZnS QDs were synthesized as follows: 0.024 g of cadmium oxide (CdO) was added to a reaction flask containing 0.44 g of stearic acid and was heated to 180 °C under inert conditions, forming a colorless solution. The solution was allowed to cool, and afterward 5 g of trioctylphosphine oxide (TOPO) and 2 g of octadecylamine were added to the flask. The flask then was evacuated and filled with inert gas several times, and the solution was heated to 200–300 °C (the exact temperature depends on the desired size). A 0.2 g sample of Se was dissolved in 2–4 mL TOPO under inert conditions and then was added to the reaction flask. Finally, 0.4 mL of dimethylzinc ($\text{Zn}(\text{Me})_2$) was added to 0.07 mL hexamethyldisilathiane ($(\text{TMSi})_2\text{S}$) under an inert atmosphere and then was added to the reaction flask. The reaction time could range from minutes to hours depending on the desired size of the nanocrystals. Finally, the solution was allowed to cool, was dissolved in trichloromethane (CHCl_3), and was precipitated with methanol (MeOH). The precipitate was collected by centrifugation and was washed several times with MeOH. These TOPO passivated nanocrystals were then dispersed in the desired solvent, including toluene, CHCl_3 , and hexane.

For solubilization: 20 mg of mercaptosuccinic acid (MSA) and 20 mL of MeOH were placed in a 50-mL three-neck flask. The pH of the solution was adjusted to 10.6 with tetramethylammonium hydroxide pentahydrate ($(\text{CH}_3)_4\text{NOH}\cdot 5\text{H}_2\text{O}$). Ten milligrams of as-prepared TOPO-capped CdSe/ZnS core/shell QDs was added to the solution. The solution was heated at 65 °C with magnetic stirring for 6 h under Ar protection. Then the solution was cooled down to room temperature. Excess ether was added to precipitate the resulting water-soluble QDs. After centrifugation and decantation, deionized water was added to obtain an aqueous solution of the CdSe/ZnS core/shell QDs. The QD520s were conjugated to streptavidin by using the activator 1-ethyl-3-(3-dimethylaminopropyl) carbodiimide hydrochloride (EDC). Each 1 mL reaction in phosphate buffered saline (PBS) contained 1–2 mg of EDC, 0.025–1 mg of protein, and 200 mL of the solubilized QD solution with OD = 0.1 at the exciton peak. Conjugation was for 2 h in the dark, unless otherwise stated, and unbound conjugate was removed by dialysis or centrifugation and washing in dH_2O . Formation of

amide bond linkages was confirmed by Fourier transform infrared spectroscopy (FTIR).

QDs measured by FCS were diluted in HPLC water to achieve between 1 and 30 particles within the observation volume (roughly a dilution factor of 1:50 to 1:5000). Between three and five hundred runs (using an automated system) were performed at each laser intensity and excitation condition. At intensities higher than ~147 kW/cm^2 (~166 μW of 488 nm at the sample), the QD520 and QD560 solution was additionally diluted 5-fold and 10-fold respectively in HPLC water to ensure safety to the detector and the experiments were continued. FCS experiments were also performed on HPLC water at various intensities from ~6.5 to 1030 kW/cm^2 (~2–1100 μW at the sample; data not shown) to ensure any contributions to the signal from the environment of the QDs as well as the background signal from the lab were minimal. All FCS experiments took place in a virtually dark room to minimize background. Power exiting the argon laser was approximately 10.5 mW and was varied using optical density filters. The power at the sample was measured using a New Focus 3803 (San Jose, CA) or PM120 (Thorlabs, Newton, NJ) power meter.

For calibration of the FCS system, autocorrelations were measured under the same conditions as the QDs. Autocorrelation data for replicates within each group of experimental runs was obtained, averaged, and then fitted as previously described. Sudden increases of more than 10% in the average fluorescence intensity due to aggregates in the sample resulted in unusable autocorrelation curves; because of this problem, curves which deviated by more than 2 standard deviations from the mean of the autocorrelation obtained under a given set of conditions were analyzed separately and usually did not yield a good fit with any analytical fitting function. The frequency and magnitude of such fluorescence bursts also were quantified under similar experimental conditions.

Assay for QD Aggregation in Saline Solution. Solutions of 10, 20, 50, 75, and 100 mM NaCl were made by dilution of a 1 M NaCl stock in HPLC water. An aliquot of QD520s as received from lab synthesis was diluted 1:50 with HPLC water, followed by 30 s of vortexing, and then was added to and mixed with the aqueous NaCl for a final dilution of 1:200 and a volume of 200 μL . After addition, QDs were allowed to freely diffuse for 1 min before FCS data acquisition. Samples were illuminated by ~13 μW at 488 nm. FCS data was captured at 10 s per run for 100 runs for each sample with average fluorescence count rates calculated every 0.105 s.

Numerical Modeling of the FCS Observation Volume. Numerical simulation of the FCS observation volume was carried out using methods presented previously.^{27,28} Briefly, the illumination volume was simulated for a 1.2 NA water infinity-corrected objective with underfilled back aperture (underfilling factor 2, equal to the ratio of the back aperture radius to the incoming assumed Gaussian laser beam $1/e^2$ radius). For the collection efficiency profile $\Omega(\vec{r})$, the diffraction-limited point spread function for the same objective was convolved with the detector aperture, a circle of radius 5 optical units, which is close to but slightly larger than the value that gives the best signal-to-noise ratio for FCS²⁷ and also a reasonable estimate of the experimental value of ~5.8 optical units. The position \vec{r} is measured from the focus. The radius in optical units (r_d) is calculated using $r_d = 2\pi \cdot \text{NA} \cdot R_d / \lambda M$ where R_d is the detector aperture radius in real space, NA is the objective lens numerical aperture, λ is the emission wavelength, and M is the overall magnification. $\Omega(\vec{r})$ describes the relative probability of collecting a photon emitted from a given point \vec{r} in the sample.

TABLE 1: Excitation, Emission, and Diffusion Properties of QDs and Alexa 488

fluorescent probe	λ_x (nm)	λ_d (nm)	D (m ² /s) $\times 10^{-12}$	r_H (nm)	ϵ (M ⁻¹ cm ⁻¹) $\times 10^5$
T2-496	405	440-550	10.1 \pm 0.4	22.7 \pm 1.8	0.45 ^a
QD520	488	505-570	8.9 \pm 1.4	24.8 \pm 3.8	30
QD560	514	550-630	30.6 \pm 2.8	7.6 \pm 1.2	43
Qdot565	514	550-630	15.9 \pm 0.9	13.9 \pm 0.8	1.22 ^b
Rhodamine B	514	550-630	290 ^c		
Alexa 488	488	505-570	250 ^d		0.73 ^e

^a Provided by the manufacturer, Evident Technologies, Troy, NY. ^b Using the concentration provided by the manufacturer, Quantum Dot/Invitrogen, Corp., Carlsbad, CA. ^c Measured by FCS under 488 nm excitation in methanol using Alexa 488 as a reference. ^d Ref 46. ^e Excited at 494 nm in water, provided by the manufacturer, Molecular Probes/Invitrogen, Eugene, OR.

The observation volume at low intensity was then calculated using $O(\vec{r}) = [I(\vec{r})]/[\Omega(\vec{r})]$, where $I(\vec{r})$ is the illumination intensity. For finite intensity, the distortion of the observation volume was modeled using the equation

$$O_s(\vec{r}) = \frac{[O(\vec{r})][I(\vec{r})/I_{\text{sat}}]}{1 + I(\vec{r})/I_{\text{sat}}} \quad (4)$$

where $O(\vec{r})$ and $O_s(\vec{r})$ are the observation volume profiles in the absence and presence of saturation effects, respectively, and I_{sat} is a characteristic saturation illumination intensity.²⁹ The time-averaged collected fluorescence F_{tot} was calculated by previously described methods³⁰

$$F_{\text{tot}} = \chi \int O(\vec{r}_o) \langle C(\vec{r}_o) \rangle d^3 \vec{r}_o \quad (5)$$

where C is the concentration, \vec{r}_o is the position in object space, and χ is a multiplicative constant proportional to the overall detection efficiency. The time-averaged number of molecules (N) within the observation volume at a given concentration C is calculated by

$$N = CV = C \left[\int W(\vec{r}) d\vec{r} \right]^2 \left[\int W^2(\vec{r}) d\vec{r} \right]^{-1} \quad (6)$$

where $W(\vec{r})$ is $O_s(\vec{r})$, normalized to unity at its maximum, and V is the total volume defined by $O_s(\vec{r})$.²⁷ Then, count rate per molecule $\eta = F_{\text{tot}}/N$. Once $O_s(\vec{r})$ was calculated, the autocorrelation $G_D(\tau)$ was determined for the case of three-dimensional (3D) diffusion by convolution of $O(\vec{r})$ with the normalized Green's function for diffusion,

$$\Psi(\vec{r} - \vec{r}', \tau) = \frac{1}{(4\pi D\tau)^{3/2}} \exp\left[-\frac{|\vec{r} - \vec{r}'|^2}{4D\tau}\right] \quad (7)$$

multiplication by $O_s(\vec{r}')$, and integration to obtain an expression

$$G_D(\tau) = \int \int d\vec{r} d\vec{r}' O(\vec{r}) \Psi(\vec{r} - \vec{r}', \tau) O_s(\vec{r}') \quad (8)$$

for the diffusion autocorrelation.²⁷ The calculated autocorrelation then was fitted using the standard fitting function from literature for 3D diffusion (eq 1 with $F_i = 0$), to determine the changes in expected fitting parameters that resulted from the distortion of the observation volume by fluorescence saturation. In particular, the diffusion time $\tau_D^{(\text{calc})}$ and its inverse $k_D^{(\text{calc})} = 1/\tau_D^{(\text{calc})}$ are determined from the fits of the calculated $G(\tau)$. We calculated and analyzed $G_D(\tau)$ as a function of I_0/I_{sat} , where $I_0 = I(\vec{r})$ evaluated at $\vec{r} = 0$, for 61 values of I_0/I_{sat} ranging from 10^{-2} to 10^4 .

Results

QD nanoparticles are being increasingly used for biological applications in living cells. However, for optimal use of such

probes, photophysical characterization of freely diffusing QDs in relevant solution environments is necessary. Four types of QDs were characterized in this study: two laboratory-manufactured CdSe/ZnS dots emitting nominally at 520 nm (QD520) and 560 nm (QD560), and two commercially synthesized CdSe/ZnS dots, Evident Technologies Lake Placid Blue Type II EviTags (abbreviated T2-496) and Quantum Dot Corporation QD565 amino PEG QDs (abbreviated Qdot565). Because the QD520s and QD560s were synthesized by similar methods, but the T2-496 and Qdot565 dots were prepared by different (proprietary) methods, direct comparisons between QDs will be limited to the QD560s and QD520s, which differ only by the emission wavelength and a streptavidin coating applied to the QD520s, which was not applied to the QD560s. Using FCS, samples were characterized in aqueous solution for brightness, diffusion coefficient, fluorescence flicker, concentration, and aggregation in saline (NaCl) solution.

FCS Measurements at Low Intensity: Diffusion Coefficient and Hydrodynamic Radius. Diffusion coefficient (D) and hydrodynamic radius (r_H) of the QDs were determined using $D = r_0^2/4\tau_D$, where τ_D is the diffusion time from FCS and r_0 is the $1/e^2$ radius of the observation volume. Values of the beam waist were calculated using a dye with known diffusion coefficient, such as Rhodamine B or Alexa 488. Alexa 488 and Alexa 546 were used as a calibration for Qdot565s. Experimental values were checked using (1) the analytical form from Pawley,³¹ $(r_0)\sqrt{2 \cdot \ln 2} = \text{FWHM} = 0.55 \lambda/\text{NA}$, where NA is numerical aperture, and λ is wavelength, and (2) a numerical simulation of the focal volume optics in confocal FCS following methods described previously³⁰ that takes into account the numerical aperture ($\text{NA} = 1.2$), excitation and detection wavelengths, objective back aperture overfilling ($r_{\text{beam}}/r_{\text{BA}} \sim 0.5$ at 488 and 514 nm; $r_{\text{beam}}/r_{\text{BA}} \sim 0.25$ at 405 nm), the detector aperture ($\sim 50 \mu\text{m}$ optical fiber), and the magnification ($60\times$). Experimental values for the beam waist tended to be underestimated by the expression from Pawley, but agreed reasonably well with the values predicted by the simulations (data not shown). Table 1 shows measured values of D and r_H and the wavelengths of excitation (λ_x) and detection (λ_d). The effective hydrodynamic radius r_H was determined using the Stokes-Einstein equation $D = k_B T/6\pi\nu r_H$ where $k_B T$ is Boltzmann's constant times temperature ($T \sim 300$ K), D is the measured diffusion coefficient, and the viscosity $\nu = 1 \times 10^{-3} \text{ kg}\cdot\text{m}^{-1}\cdot\text{s}^{-1}$ in water.³²

Concentration and Extinction Coefficient. The concentrations of QD520s and QD560s were determined relative to an Alexa 488 or Rhodamine B sample, respectively, of known concentration under the same excitation conditions. Figure 1A shows measured absorbance spectra for the three QD samples, normalized to unity at 350 nm for presentation purposes. The emission spectra are shown in Figure 1B and reveal significantly narrower spectra ($1/e^2$ half-width) for the QDs compared to the

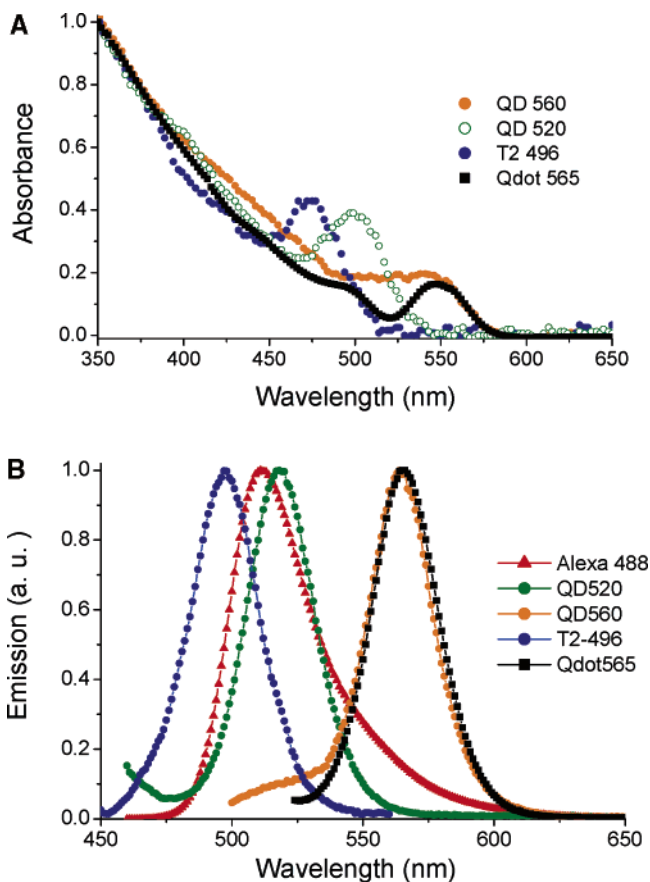


Figure 1. Absorbance (A) and emission (B) spectra of samples of T2-496 (blue circles), QD520 (green circles), QD560 (orange circles), and Qdot565 (black squares) QDs, and Alexa 488 (red triangles).

Alexa 488, yielding 27.1, 26.7, and 27.5 nm for the T2-496, QD520, and QD560 dots, respectively, compared with 40 nm for Alexa 488. The Alexa 488 concentration was determined from the absorbance $C = A/\epsilon L$ and was consistent with the value expected from the known mass of dye in a known volume of water. The extinction coefficient of the QD sample ϵ_{QD} is then given by $\epsilon_{\text{QD}} = A_{\text{QD}}/L_{\text{QD}}C_{\text{QD}}$ and for the reference $\epsilon_{\text{Ref}} = A_{\text{Ref}}/L_{\text{Ref}}C_{\text{Ref}}$ where the concentration of molecules C was determined from FCS using eq 3. Then the rearrangement of these two equations gives $\epsilon_{\text{QD}} = \epsilon_{\text{Ref}}A_{\text{QD}}L_{\text{Ref}}C_{\text{Ref}}/A_{\text{Ref}}L_{\text{QD}}C_{\text{QD}} = \epsilon_{\text{Ref}}A_{\text{QD}}C_{\text{Ref}}/A_{\text{Ref}}C_{\text{QD}}$ with equal absorbance path lengths for the reference and QDs. This analysis assumes that all of the QDs that absorb at the excitation wavelength also are fluorescent (either steadily or intermittently) when excited at the same wavelength and detected using our combination of fluorescence filters. This assumption introduces an uncertainty in the extinction coefficient that we estimate to be of order 2-fold, using the measured estimates of the percentage of QDs which are absorbing and nonfluorescent compared with absorbing and fluorescent from Yao et al., who also characterized QDs made with the same core and cap.³³ The value of the extinction coefficient of Alexa 488 was taken from the manufacturer (see methods). Table 1 shows values of ϵ for QDs determined in this way.

FCS at High Excitation Intensity: Development of a New FCS Fitting Function. As excitation intensity was increased, the standard analytical fitting function from literature (eq 1) was able to describe the autocorrelation of Alexa 488 (Figure 2) under all attempted excitation conditions, allowing interconversion between the bright state and one dark state (i.e., eq 1 with $m = 1$). However, the autocorrelation of QDs at high-

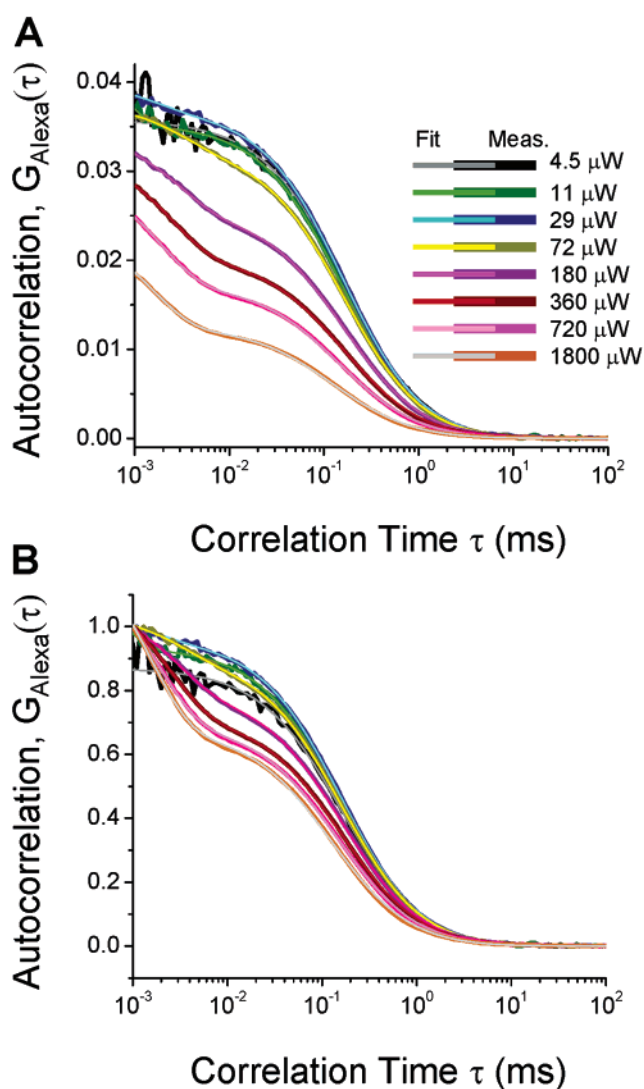


Figure 2. (A) Autocorrelation curves $G(\tau)$ of Alexa 488 as a function of excitation intensity at the sample. The power at the sample is shown in the legend next to the corresponding measured (thick line) and fitted (thin line) autocorrelation. Note the consistent progression of the correlation toward lower amplitude as intensity increases and the distinct shoulder in the autocorrelation for $\tau < 10 \mu\text{s}$ at the highest excitation intensities. (B) Alexa autocorrelation curves normalized to illustrate the changes in the functional form of $G(\tau)$. The same legend applies as for panel (A).

intensity could not be described sufficiently well (see example in Figure 3 of fit using eq 1 allowing interconversions between one bright and two dark states, labeled *Standard Fit*, the standard fitting function from literature). To extract reliable, meaningful information from the measured $G(\tau)$, it was necessary to develop a new fitting function

$$G_{\text{QD}}(\tau) = \left(\frac{1}{N}\right) \frac{1}{1 + \tau/\tau_{\text{D}}} \frac{1}{(1 + \tau/\omega^2\tau_{\text{D}})^{0.5}} \times \prod_{n=1}^5 \frac{1 - \alpha^{n-1}F_1 + \alpha^{n-1}F_1 e^{-\beta^{n-1}R_1\tau}}{1 - \alpha^{n-1}F_1} \quad (9)$$

where N , τ_{D} , and ω are the number of molecules, diffusion time, and axial-to-lateral width ratio of the observation volume, respectively, as in eq 1, F_1 and R_1 are the occupancy and sum of forward and reverse interconversion rates, respectively, for the first dark state, and α and β are constants connecting the

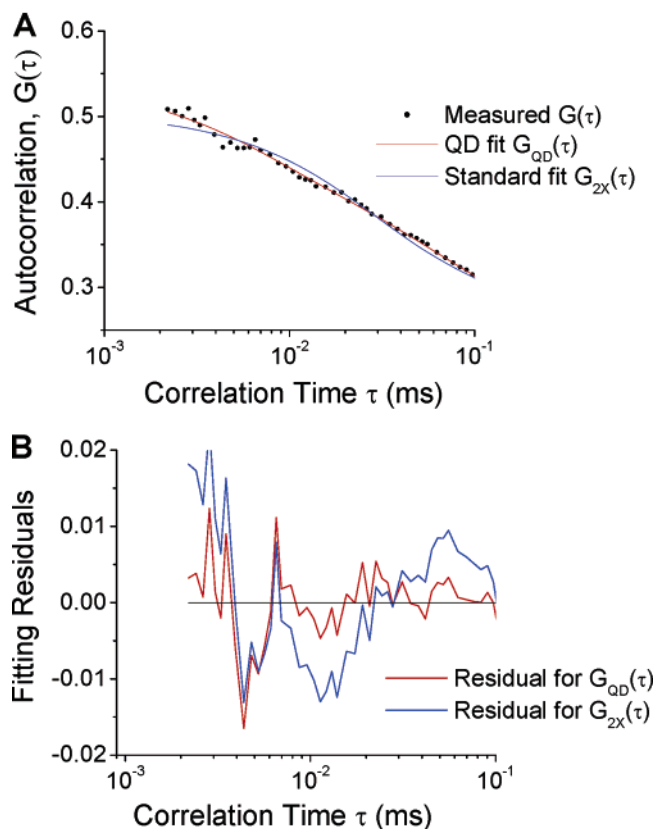


Figure 3. Quantitative comparison of fitting functions used to describe the measured autocorrelation of QD nanoparticles in vitro. (A) Measured autocorrelation (black dots) for QD520s at high intensity ($\sim 8 \times 10^{23}$ photons/cm²·s at the sample) is poorly described by the standard fitting function from literature with 3D diffusion, one bright state, and two dark states (blue line), but is well described by an autocorrelation function that incorporates diffusion, multiple dark states, and the same number of free parameters (red line). (B) The residuals corresponding to the two fitting functions shown in (A): the deviation between fit and measurement is larger using the diffusion plus one bright and two dark states (blue line; residual for $G_{2x}(\tau)$) than for the multiple dark state model (red line; residual for $G_{QD}(\tau)$).

fractions and rates, respectively, of all of the other dark states to F_1 and R_1 . This function was designed to accommodate a large number of dark states with a distribution of off-times that varies as the inverse power of the off time (i.e., a positive power of the interconversion rate), as has been reported previously in literature.²⁰ The new function allows one bright state and five dark states (which would otherwise yield an unwieldy 14 free parameters) but builds in the power-law distribution of off times by relating the amplitude and rates of the dark states by a pair of multiplicative constants: α , which describes the occupancy of the n^{th} dark state relative to the $(n - 1)^{\text{th}}$ dark state, and β , which describes the ratio of R_n (the sum of forward and reverse interconversion rates of the n^{th} dark state) to R_{n-1} for the $(n - 1)^{\text{th}}$ dark state. Thus, for $\alpha = 0.5$, the second dark state will have half the amplitude of the first, and for $\beta = 5$, the sum of forward and reverse interconversion rates of the second dark state will be $5R_1$ and for the third dark state will be $25R_1$. This relationship between the rate constants and dark state occupancies limits the number of free parameters to eight (the same number as the standard FCS fitting function for 3D diffusion plus two interconversions between a bright and two dark states). Addition of a larger number of dark states did not significantly improve fits (data not shown). Figure 3 shows a comparison of fits using eq 1 and eq 9 with the same number of fitting parameters. Note the significantly improved fits using eq 9

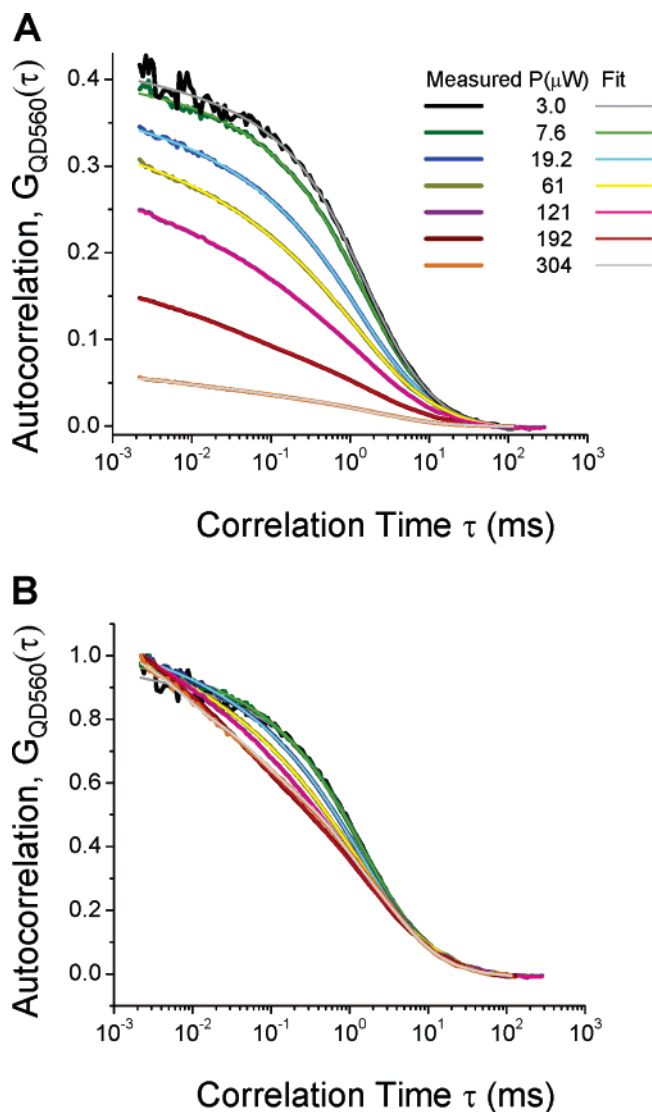


Figure 4. (A) Autocorrelation $G(\tau)$ and (B) normalized autocorrelation of QD560s as a function of excitation intensity at the sample. The power at the sample is shown in the legend next to the corresponding measured (thick line) and fitted (thin line) autocorrelation. The shape of $G(\tau)$ is qualitatively different from that of Alexa at high intensity, showing a more nearly linear behavior at small values of τ (plotted with a logarithmic horizontal axis). This linear behavior is indicative of the deviation of the measured correlation from the standard analytical functional form for interconversions between a bright state and one or two dark states.

(curve labeled *QD fit* in Figure 3). Figure 4 shows examples of the autocorrelation of QD560 fluorescence, fitted using eq 9 for a variety of intensities.

It should be noted that this new functional form (eq 9) reduces to the standard analytical form (eq 1) of 3D diffusion plus one exponential (chemical kinetic) component in the limiting case where $\alpha \rightarrow 0$. In the limit, as β becomes large (i.e., a system where R_1 and R_2 differ by a large factor in time scale), eq 9 also reduces to eq 1 with one bright and two dark states if the only rates within the accessible experimental time window are R_1 and R_2 . The total fraction of dark molecules (F_{dark}) is calculated using

$$F_{\text{dark}} = 1 - \frac{N_{\text{bright}}}{N} \quad (10)$$

where N is the total number of molecules obtained from the fit of $G(\tau)$ using eq 9, and $N_{\text{bright}} = 1/G_{\text{fit}}(\tau_0)$ where $\tau_0 = 10^{-6}$ s.

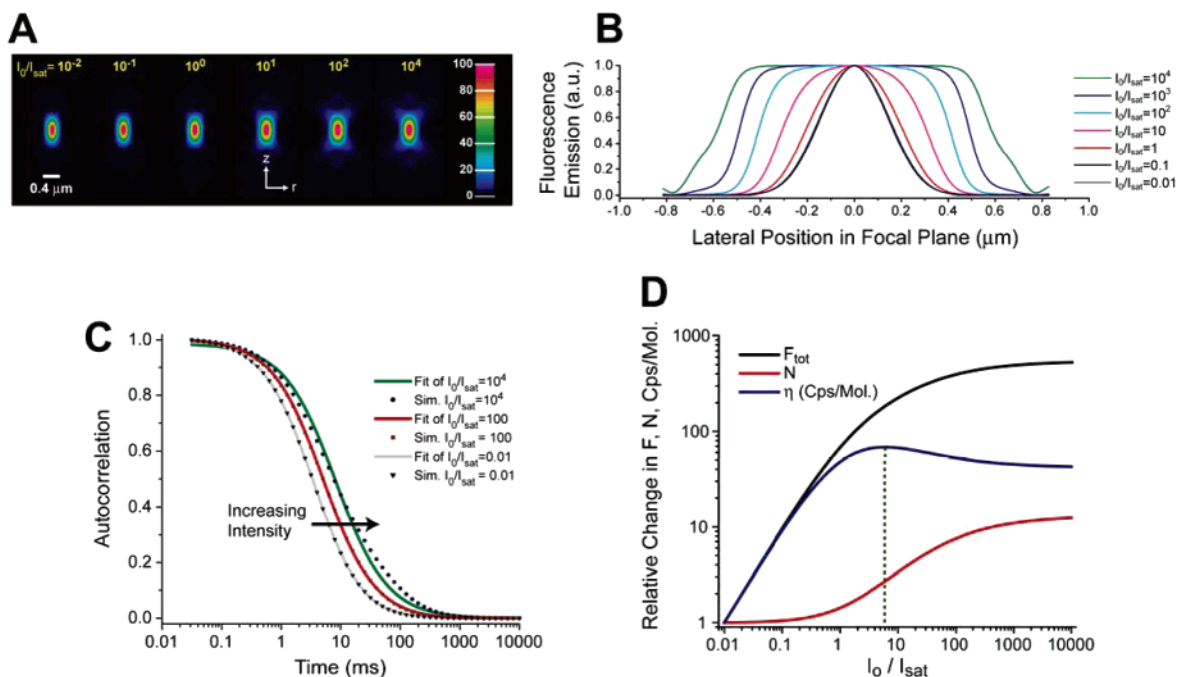


Figure 5. Effect of high (near saturating) illumination intensity on the FCS autocorrelation function and expected FCS parameters. (A) Fluorescence emission profiles calculated using diffraction theory^{28,30} and plotted with linear pseudocolor scale as a function of I_0/I_{sat} , the ratio of peak intensity (I_0) to saturating intensity (I_{sat}). (B) Fluorescence emission profiles plotted as a function of lateral position in the focal plane. Significant distortions in the observation volume occur, especially at intensities above $I_0/I_{sat} \sim 10$. Profiles were normalized to unity at the focus. (C) Effect of increased intensity on the expected FCS diffusion autocorrelation. At low intensity, the autocorrelation calculated by simulations (black triangles) is well described by the standard analytical fitting function for 3D diffusion only (eq 1 with $F_i = 0$, gray line). At moderately high-intensity $I_0/I_{sat} \sim 100$ (red squares) using a detector aperture close to the value for maximum signal-to-noise ratio, the calculated autocorrelation still can be fitted by eq 1 (red line), but the diffusion time is significantly (~ 1.5 -fold) higher. At very high-intensity $I_0/I_{sat} \sim 10^4$, the observation volume is strongly distorted and the calculated autocorrelation (black circles) can no longer be described by the standard fitting function (green line). Failure of the standard fitting function occurs beginning around $I_0/I_{sat} \sim 130$. (D) log-log plot of calculated total fluorescence intensity (F_{tot} , black line), number of molecules (N , red line), and count rate per molecule (η , blue line), which depend strongly on illumination intensity. At low intensity, F_{tot} and η depend linearly on intensity (slope of 1 on the log-log plot), and N is independent of intensity. At modest intensity, N increases slightly with intensity while F increases with slope < 1 , leading to a maximum in η at $I_0/I_{sat} \sim 6$. Further increase in I_0/I_{sat} leads to a strong increase in N with a more modest increase in F , yielding a reduced η . At intensities below $I_0/I_{sat} \sim 100$, the standard fitting function may be used to analyze measured autocorrelation if parameters are interpreted with extreme caution. This intensity corresponds to approximately 20-fold above the intensity $I_0/I_{sat} = 6$ at which η is expected to be maximum. Inability to fit measured autocorrelations below this intensity using the standard diffusion fitting function may result from factors other than saturation, such as misaligned optics, spherical aberrations, fluorescence kinetics on millisecond and microsecond timescales, or nonstandard diffusion.

At the lowest illumination intensities, the QD autocorrelation curves cannot be fitted using pure diffusion (eq 1 with $F_i = 0$). Even from visual inspection of the autocorrelation and fit, the QD autocorrelation requires accommodation of dark states. Equation 1 could be used at low-intensity if transitions between a bright and two dark states were allowed. For powers at the sample below $\sim 10 \mu\text{W}$, the χ^2 values for the new (eq 9) and standard fitting functions (eq 1) were comparable. However, above this power level, the χ^2 values were consistently more favorable for the new function. Overall, including the complete range of sample powers, the maximum χ^2 for the new function was 0.810 compared to 1.138 for the standard function.

Numerical Modeling of the FCS Observation Volume and Autocorrelation at Intensities Near Saturation. To determine whether distortion of $O(\bar{r})$ by saturation could explain the altered form for the autocorrelation, $O(\bar{r})$ was calculated for the known experimental system as a function of illumination intensity. The spatial profile of $O(\bar{r})$ without a detector aperture is shown in Figure 5A,B as a function of I_0/I_{sat} , the ratio of the peak intensity to saturation intensity. Including a detector aperture of 5 optical units, the calculated autocorrelation (Figure 5C) is shown as a function of I_0/I_{sat} , demonstrating that at low intensity and intensities up to $I_0/I_{sat} \sim 100$, $G(\tau)$ can be described by just the diffusion part of $G_X(\tau)$ (eq 1 with $F_i = 0$), but as I_0 increases, the diffusion time also increases (Figure 5C). Above $I_0/I_{sat} \sim$

130, distortion of $O(\bar{r})$ becomes so strong that the standard analytical fitting function can no longer describe the calculated $G(\tau)$. Above this intensity, interpretation of results analyzed with eq 1 will be problematic.

To provide comparison with standard experimental quantities measured by FCS, F_{tot} and N also were calculated using the same $O(\bar{r})$ used to calculate the autocorrelation (Figure 5D). Note that on a log-log plot, F_{tot} increases linearly (slope 1) at low intensity and less rapidly as saturation becomes significant. As expected, N is relatively constant at low intensity, but increases drastically at higher intensities. At even higher intensities, the confocal detector aperture partially limits the growth in N , resulting in a shallower slope as a function of intensity. The ratio $\eta = F_{tot}/N$ was also calculated as a function of I_0/I_{sat} , and shows a distinct maximum at $I_0/I_{sat} \sim 6$ under our experimental conditions. At this illumination intensity and up to $I_0/I_{sat} \sim 100$, we expect that for a fluorophore undergoing simple 3D diffusion, eq 1 can be used to analyze the measured diffusion autocorrelation. At intensities more than ~ 16 -fold higher than the maximum in η , the distortions in $O(\bar{r})$ will be so strong that eq 1 can no longer be used and interpretation of results will be difficult. On the other hand, at intensities well below $I_0/I_{sat} \sim 100$, the inability to fit the measured autocorrelation using eq 1 likely indicates that effects other than saturation are causing the deviation. Experimental evidence of

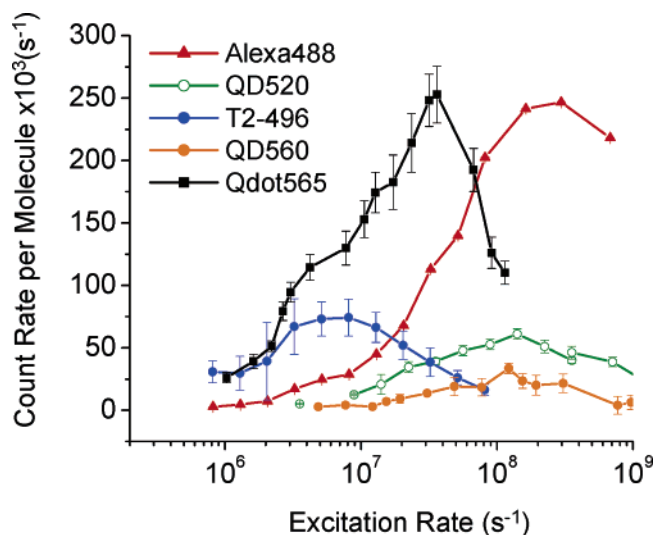


Figure 6. Measured brightness per particle (e.g., count rate per molecule, η) as a function of excitation rate (k_x) for Alexa 488 (red triangles), T2-496 dots (filled blue circles), QD520s (open green circles), QD560s (filled orange circles), and Qdot565s (filled black squares), corrected for the wavelength-dependent dichroic mirror and fluorescence emission filter transmission efficiencies. Surprisingly, the QDs are typically less bright at their maximum η than Alexa 488 at its maximum, except for the Qdot565s. However, at low excitation rate, the QDs are under some conditions brighter due to their large excitation cross sections and tendency to saturate at low intensity. Error bars are standard deviation.

this condition includes the observation that the autocorrelation of Alexa488 was fitted well by eq 1 at high intensity, even at intensities beyond the maximum in η . The QDs are not well described by eq 1 under equivalent or much lower excitation intensities.

Measured Count Rate per Molecule (Brightness per Particle). While QDs show significantly better resistance to photobleaching than organic fluorophores,³⁴ also of particular interest for single molecule imaging is the molecular brightness, or the number of detected photons per second per molecule. The brightness, also referred to as η , was determined using the background-corrected average fluorescence count rate divided by the background-corrected number of molecules: $\eta = F/N$. Figure 6 shows brightness as a function of excitation rate for the QD520, QD560, Qdot565, and T2-496 QDs. Brightness values were corrected for the measured dichroic and emission filter transmission efficiencies as a function of wavelength, using the measured dye and QD emission spectra. The maximum brightness η_{\max} was $(74 \pm 15) \times 10^3 \text{ s}^{-1}$ for the T2-496 (blue) dots at $k_x \sim 8.1 \times 10^6 \text{ s}^{-1}$, $\eta_{\max} \sim (61 \pm 4) \times 10^3 \text{ s}^{-1}$ at $k_x \sim 1.4 \times 10^8 \text{ s}^{-1}$ for the QD520s, $\eta_{\max} \sim (253 \pm 23) \times 10^3 \text{ s}^{-1}$ at $k_x = 3.6 \times 10^7 \text{ s}^{-1}$ for the Qdot565s, and $\eta_{\max} \sim (24 \pm 8) \times 10^3 \text{ s}^{-1}$ at $k_x \sim 1.5 \times 10^8 \text{ s}^{-1}$ for the QD560s. Note the trend of increasing brightness (comparing QD520s and QD560s) as the emission wavelength decreases. The T2-496 dots follow the same trend, but the Qdot565s do not; both are synthesized by a different method, so variables other than emission wavelength likely also result in the differences. It is also possible that the streptavidin coating on the QD520s also enhances the brightness relative to the QD560s. It should be noted that the T2-496 dots were measured exciting at 405 nm with an underfilled ($\beta \sim 4$) objective back aperture, which will reduce the collection efficiency compared to the measurements at 488 nm ($\beta \sim 2$) by approximately (3.0 ± 0.5) -fold based on theoretical calculations. Correcting for this effect, it is expected

that the T2-496 dots excited at 405 nm will be similar in brightness to Alexa 488 excited at 488 nm.

The observed maximum brightness yields (in our system) at maximum ~ 650 collected photons per particle per diffusion time for the Qdot565s, ~ 340 for the T2-496 dots, 290 for the QD520, and 40 for the QD560. Similarly, in a confocal microscope in which the dwell time per pixel might be only $\sim 1 \mu\text{s}$, the number of collected photons per QD would be significantly smaller than unity, requiring a relatively large number of QDs to be present in the observation volume (typically $\sim 10^{-15} \text{ L}$) to ensure enough collected photons for shot noise statistics not to dominate the fluorescence signal. On the other hand, because the photobleaching resistance of the QDs is significantly better than for most organic dyes¹¹ (Alexa 488 already being a fairly photobleaching-resistant example), if one is willing to collect data over longer timescales, a significantly larger number of photons can ultimately be collected.

Quantification of Fluorescence Intermittency. One of the key parameters limiting the fluorescence brightness in QDs has been their tendency to undergo fluorescence intermittency (i.e., flicker on microsecond and millisecond timescales and blinking on timescales of $> 100 \text{ ms}$). We found that a significant fraction of the QDs are in dark states at any given time, and we analyzed the FCS autocorrelation using a new form for $G(\tau)$ developed specifically to describe QD photophysics (eq 9). Figure 7A shows the fraction of QDs found in a dark state as a function of intensity ratio $I/I_{\eta_{\max}}$ where $I_{\eta_{\max}}$ is the intensity at which η is maximum. At $I/I_{\eta_{\max}} = 1$, the QD560s had the largest fraction in the first dark state, followed by the QD520s and T2-496 dots, and the Qdot565s had the smallest fraction in the first dark state, which is consistent with the higher brightness of the Qdot565s.

Next, we examined the relative rates for interconversion between the bright and dark states. Figure 7B shows R_1 , the interconversion rate between the bright state and the first dark state (equal to the sum of forward and reverse reaction rate constants). The trend observed is consistent with the large fraction of QDs in dark states: the rates are one to two orders of magnitude slower than for Alexa 488. Furthermore, the QDs that have the highest F_1 fractions (i.e., QD560s) also have the slowest interconversion rates, and the QDs which have the highest peak molecular brightness (Qdot565s) also had the fastest interconversion rates. Thus, the fact that QDs spend a significant fraction of their time in dark states strongly limits their average brightness per particle.

To investigate the mechanism by which the QDs become “stuck” in dark states, several variables were examined. First, the excitation light intensity was varied. As excitation intensity increased, typically a larger fraction of QDs were found in dark states, while the rate of interconversion between bright and dark states (R_1) usually increased, except in the case of the Qdot565s. Second, reduction of oxygen concentration (by bubbling the solution continuously with Ar gas for 20 min) did not cause a significant change in the autocorrelation of QD520s, but did alter the interconversion rate of Alexa 488 between bright and dark states (data not shown).

Because the dark state population was observed to be strongly light-dependent, the total fraction of dark molecules was determined as a function of η . At low intensity (in the absence of saturation), η is expected to increase linearly with increasing intensity: $\eta \sim \gamma k_x$. As intensity increases, however, η will increase less rapidly than γk_x , and the ratio $\rho = \eta_{\text{meas}}/\gamma k_x \leq 1$ typically. As intensity increases further, ρ decreases as saturation

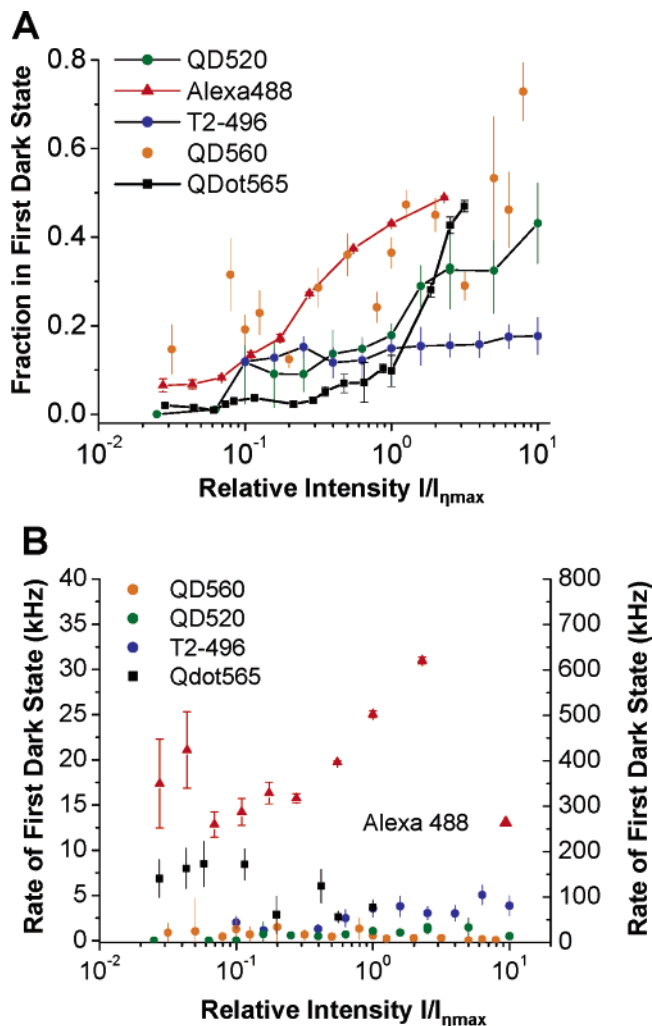


Figure 7. Intensity-dependence of dark state flicker interconversion rates and dark state occupancies in QDs. (A) A large intensity-dependent fraction of QDs is dark, especially at high intensity. T2-496 dots (filled blue circles), QD520s (filled green circles), QD560s (filled orange circles), Qdot565s (filled black squares), and Alexa 488 (red triangles) all interconvert with dark state(s) on microsecond and millisecond timescales. The highest dark fraction was observed for the QD560s and for Alexa 488, while an intermediate fraction was observed for QD520s and the smallest fraction was observed for the Qdot565 dots. The high fraction of dots in QDs correlates with a decreased interconversion rate between the bright and dark state(s), as shown in (B) where the Qdot565 (black squares; left axis) and T2-496 dots (filled blue circles; left axis) have the fastest rate among QDs, followed by the QD520s (filled green circles; left axis), and then the QD560s (filled orange circles; left axis) at $I/I_{\eta_{\max}} = 1$. However, the Alexa 488 (red triangles; right axis) shows the highest interconversion rates and also the highest peak brightness per particle. For comparison among data sets, intensities are plotted as a function of $I/I_{\eta_{\max}}$, the ratio of excitation intensity to the intensity where the peak η value was obtained. Error bars are standard deviation.

effects become more significant, with $\rho \ll 1$ at and above the maximum for η . The slope γ was determined experimentally, typically ranges from 0.002–0.03, and is related to the overall detection efficiency. Figure 8A shows F_{tot} versus ρ for the QDs in this study. The value of F_{tot} indeed decreases as a function of ρ for all QDs examined. To quantify the observed decrease, F_{tot} was least-squares fitted using an exponential decay: $F_{\text{tot}} = A_1 e^{-k\rho}$, where A_1 is a constant. The resulting fits are shown in Figure 8A. The value of k was found to correlate strongly with the peak brightness (maximum value of η) of a given type of QD, as is shown in Figure 8B.

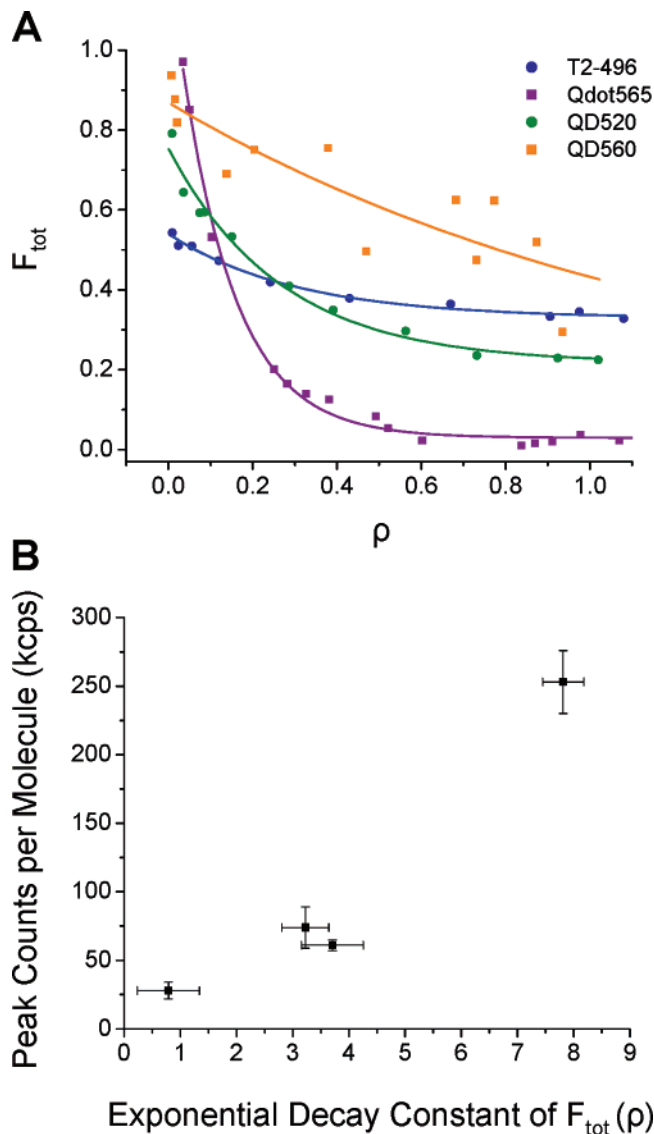


Figure 8. Dark states limit count rate per molecule (η) in QDs. (A) The total fraction of dark QDs, as determined by FCS, is shown as a function of ρ , the ratio of measured η to expected η . The expected η (what could be obtained in the absence of saturation) was determined by fitting the linear low-intensity dependence of η vs excitation rate, and extrapolating that linear dependence to high intensity. For all QDs measured, the fraction of dark QDs increases as ρ decreases. (B) The QDs with the highest peak η had the largest exponential decay constant for F_{tot} as a function of ρ .

Effect of Biologically Relevant Ions on QD Photophysics.

Because QDs are of such interest as labels for biological systems, the photophysics of these probes must be studied as they diffuse in biologically relevant solutions. We examined the effect of adding NaCl to an aqueous solution of T2-496 dots and QD520s to simulate their use to label cells in saline solution. T2-496 dots immersed in 0.095 M NaCl did not show any significant reduction in fluorescence intensity or alteration of the emission spectrum over a period of ~ 1 h. However, for QD520s, several effects were observed after immersing them in aqueous NaCl solutions between 10 mM and 470 mM. Table 2 shows (at one fixed illumination intensity $k_x \sim 2.58 \times 10^6 \text{ s}^{-1} \text{ MHz}$) measurements of number of particles (N), diffusion time (τ_D), average fluorescence count rate (F), and count rate per bright particle (η).

Upon addition of a physiologically relevant concentration of NaCl, the average fluorescence count rate dropped ~ 16 -fold,

TABLE 2: Changes in Fluorescence and Diffusion Properties of QD520s in NaCl Solutions

[NaCl] (M)	N	τ_D (ms)	F (kHz)	η (kHz)
~ 0	1.62 ± 0.54	2.51 ± 1.13	36.1 ± 1.6	44 ± 62
0.095	0.26 ± 0.36	3.68 ± 2.5	5.1 ± 3.9	45 ± 260
0.47	0.14 ± 0.23	7.42 ± 16.5	2.3 ± 1.8	52 ± 166

TABLE 3: Changes in Frequency of Fluorescence Spikes in Aqueous Solutions of QD520s in the Presence of NaCl^a

[NaCl] (M)	$N_{1\sigma}$	$N_{2\sigma}$	$N_{3\sigma}$
~ 0	13.4 ± 2.6	4.2 ± 1.2	1.5 ± 0.9
0.095	9.9 ± 3.1	4.5 ± 1.4	2.3 ± 0.9
0.47	8.2 ± 3.1	4.0 ± 1.5	2.3 ± 0.9

^a Note that \pm values are the standard deviation of the frequency distribution, which is not necessarily equal to the uncertainty in the particular value itself. Analysis of variance (ANOVA) was used to determine significance of differences between the frequency distributions of fluorescence bursts, or “spikes.”

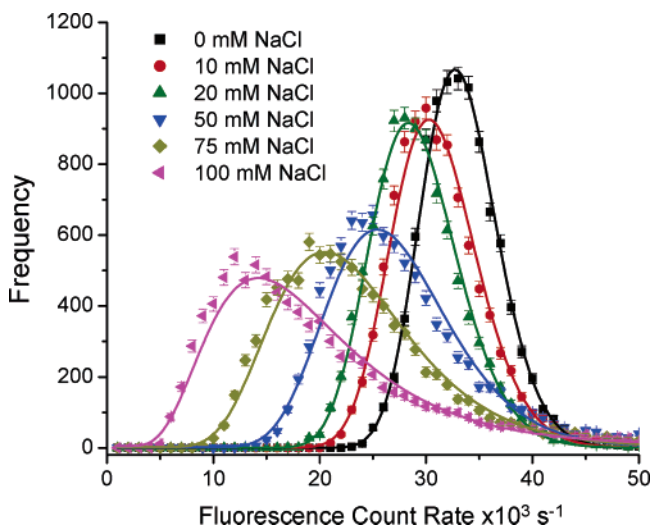


Figure 9. Brightness distributions of QD520s diluted 1:200 in HPLC water diffusing in NaCl concentrations of 10, 20, 50, 75, and 100 mM compared to a control (0 mM NaCl). The maximum count rate of the QD520s in control solution decreases to less than half when in 100 mM NaCl indicating either a growing number of aggregates or a growing number of QDs per aggregate or both with increasing NaCl concentrations.

the diffusion time increased, and the number of particles within the observation volume fell by ~ 12 -fold. Because these results are highly suggestive of an aggregation process, the brightness distribution of fluorescence fluctuations was determined and quantified: the number of “small” fluctuations $N_{1\sigma}$ (less than one standard deviation, σ , from the mean fluorescence intensity), the number of “medium” fluctuations $N_{2\sigma}$ (between 1σ and 2σ), and the number of “large” fluctuations $N_{3\sigma}$ (amplitude $> 2\sigma$) observed within a 0.1 s time bin were counted over a period of 100 s and compared in NaCl and pure HPLC water, shown in Table 3. We observed a decrease in small fluctuations ($p = 5 \times 10^{-28}$ comparing ~ 0 M NaCl with 0.47 M NaCl by ANOVA), an increase in the number of large fluctuations ($p = 1.5 \times 10^{-9}$), and no significant change in the number of medium fluctuations ($p = 0.16$) in which p is the probability that the distributions of fluorescence fluctuations come from the same distribution (the null hypothesis).

To consider all sizes of fluorescence fluctuations simultaneously, the background-corrected frequency histograms of fluorescence count rate were determined (Figure 9). As NaCl concentration was varied (10, 20, 50, 75, 100 mM), the peak fluorescence count rate decreased and the width of the peak

increased. The fluorescence intensity distributions were well described by least-squares fitting with a log-normal distribution.

Discussion

Biological fluorescence applications are frequently limited by the number of photons detected from a fluorophore within a given time. While biological applications of QDs continue to grow, QDs are currently limited by intermittency and specificity of targeting. Systematic characterization of QDs to determine which properties will help increase the number of detected photons per unit time (the count rate per molecule) is worthwhile if it can suggest strategies for improvement of QDs.

FCS is useful for such photophysical characterization of fluorescent probes; here, we compare the photophysical parameters of QDs using FCS (as did Weiss et al.),²³ exploring these properties as a function of excitation and emission energy and synthesis method, rather than the QD core material. All these dots are composed of CdSe with a ZnS capping layer. From the systematic study of four QDs with the same core and cap, we find that the QDs with the highest peak count rate per molecule have the lowest occupancies in dark states and the fastest rates of interchange with those dark states. Thus, QDs are limited in their maximum emission rate because they get stuck in dark states.

Development of an Analytical FCS Fitting Function for QDs with Fluorescence Intermittency. To analyze our FCS results quantitatively, it was necessary to develop an analytical fitting function that described the measured autocorrelation $G(\tau)$. The problem is that QDs flicker and blink (undergo fluorescence intermittency) on many timescales, and thus the standard FCS fitting functions from literature are inadequate. Short of heroic efforts to use Monte Carlo methods with significant numbers of simulation parameters to predict the autocorrelation, there remains a significant need for an analytic form. This development is further motivated by the pressing need for photophysical parameters of QDs. We now present quantitative (side-by-side) comparison of QD brightness with other fluorophores; Gao and Nie 2004³⁵ give such a comparison *in vivo*, but without correction for certain relevant factors (as is stated within their manuscript). Doose and Weiss give brightness per particle for various QDs but do not compare to rhodamine or other organic dyes under the same conditions.²² Consistent with previously published results under one-photon excitation,²³ we also had limited success fitting autocorrelation curves from QDs using a model that included 3D diffusion plus flicker between one bright state and two (dark) states of lower (zero) brightness (eq 1). Particularly at high excitation rates, this analytical form was unable to describe the observed $G(\tau)$. Thus, it was necessary to surmount the problem of fitting the FCS autocorrelation of QD fluorescence, which is highly intermittent on many timescales.

We hypothesized that contributions from a large number of states might make the description of the autocorrelation by transitions between one bright state and two dark states an oversimplification. However, because of the large number of fitting parameters, it would not be possible to describe the autocorrelation using diffusion plus transitions, for example, between ten independent states with ten independent occupancies and rates. Instead, a fitting function that incorporates the known power-law distribution of off-times of semiconductor QDs²⁰ was devised, whereby transitions between a bright state and n dark states are allowed with forward plus reverse transition rates (R_n) and occupancies (F_n) that are given by $R_n = R_1(\beta)^{n-1}$ and $F_n = F_1(\alpha)^{n-1}$. This assumption leads directly to the analytical form of eq 9, which has several advantages: (1) it reproduces the

experimental observation that $G(\tau)$ at high excitation intensity is nearly linear when plotted in the standard way as a function of $\log(\tau)$; (2) the large number of states (cooperativity) and power-law distribution of off-times is incorporated a priori into the fitting function; (3) as α approaches zero, the autocorrelation reduces to the standard analytical form of diffusion plus flicker between one bright state and one dark (or dim) state; and (4) the fitting parameters are limited in number and reflect physically interpretable quantities.

The value of α is a measure of the number of states that contribute to the observed flicker: values of $\alpha \ll 1$ indicate relatively few states contributing to the flicker (autocorrelation), while values of α approaching 1 indicate that a large number of states contribute over the observable range of timescales. The value of β reports on the relative temporal spacing of the states that contribute. Large values of β correspond to states whose residence times are spread out over a wide range of timescales, while small values of β (close to unity) concentrate the off-times over a narrow range of timescales.

We observed that this fitting function described the measured $G(\tau)$ for all QDs measured in this study, and generally had lower values of χ^2 compared to the "standard" fitting function $G_{2X}(\tau)$ with the same number of fitting parameters. Furthermore, the use of an analytical fitting function permits quantitative comparison of results for the several types of QDs measured.

Dark States Limit Maximum Brightness per Particle in QDs. Surprisingly, we observe lower maximum fluorescence brightness in some of the QDs compared with both Alexa 488 and Rhodamine B. The maximum brightness of the QDs appears to be limited by the large fraction of QDs in dark states; the relatively slow rate for interconversion between the bright and dark state(s) also implies that QDs that become stuck in a dark state may reside there for a time that is longer than for Alexa 488 in its light-induced dark state(s). Because surface trapping has been proposed as a reason for dark states in QDs,¹ it is interesting to note that differences in surface-to-volume ratio could affect interchange with (and exit from) dark states. Differences in synthesis methods also may account for the reduced residence times.

The observed long off-times can be understood if the dark states accessed by higher energy excitation show slower recombination or relaxation times. In the framework of an artificial atom description of a QD,²⁴ states become more numerous at higher energies with multiplicity $2(2/\ell + 1)$, where ℓ is the envelope-function angular momentum³⁶ and those states may have wave functions that overlap significantly less with the ground state wave function, such as in InAs QDs in which higher energy states have p-orbital character and lower-energy states have s-orbital character.³⁶ Furthermore, optical transitions have been shown to correspond to the energy spacings between the upper valence band and the lower conduction levels,³⁶ further strengthening the validity of an artificial atom description. Photon absorption events will likely lead to QDs in higher energy states with potentially different angular momenta; a p-state wavefunction will have a different angular dependence than an s-state, and therefore a reduced overlap with the state from which it originated. This reduced wavefunction overlap of high-energy states would lead to slower recombination (relaxation) rates, and if more than one state can be populated, would also lead to a distribution of relaxation rates that may decrease rapidly (perhaps exponentially) with increasing energy difference from the ground state. Such a distribution of rates is consistent with a power-law distribution of off-times, as our observed autocorrelation functions and other published experi-

mental results^{8,20} suggest. The excess energy (ΔE) provided to the system initially may serve to determine the relative fractions of the numerous accessible states; a large ΔE may result in a more evenly populated set of states, some of which have very slow rate of recombination and thus lead to long off times.

Comparison of Brightness of QDs and Organic Dyes. Numerous reports compare the brightness of QDs and organic fluorophores. Chan and Nie¹¹ and Wu et al.,¹⁸ quantitatively compare collected fluorescence intensities of QDs with Alexa and Rhodamine dyes and find significantly higher intensities for QDs. We also observe such trends under conditions of low laser intensity where the QDs are near their maximum brightness per particle (number of collected photons per particle/molecule per second) but where the organic dyes have not yet reached their maximum brightness. However, because of the fact that this brightness is dependent on excitation laser intensity (as well as extinction coefficient, fluorescence quantum yield, and detection efficiency), side-by-side comparison of QDs and organic fluorophores under the same excitation intensity will in many cases not reveal which probe is better under optimal conditions (e.g., one probe at its best may be better than another at its best). Thus, we have quantified the maximum brightness and the intensity (for a given excitation wavelength) at which this maximum is obtained, rather than just comparing collected photon flux at one intensity. We find saturation of QDs at much lower intensities than for organic dyes, and so the QD brightness is higher at low intensity, but organic dyes can go much higher in excitation intensity before saturating and thus under optimal conditions beat the brightness of some QDs at high laser power levels. Because in confocal microscopy the excitation power is usually high but freely adjustable, estimated values for the intensity level that gives maximal count rate per molecule can be used to optimize measurements using QDs and other fluorophores.

Efficient Absorption and Reduced Saturation Intensity Facilitate Observation Volume Distortions When Exciting QDs. The measured absorption cross sections for QDs (e.g., $\sim 10^{-15}$ – 10^{-14} cm²) are more than an order of magnitude larger than for organic dyes such as Alexa ($\sigma_{\text{Alexa}} \sim 2.1 \times 10^{-16}$ cm²). This is consistent with previously reported values for QDs ($\sigma \sim 4 \times 10^{-15}$ cm²)⁸ and $(0.5\text{--}4) \times 10^6$ M⁻¹ cm⁻¹ (equivalent to $\sim (1.4\text{--}12) \times 10^{-15}$ cm²)^{5,9,37} and approximately an order of magnitude larger than reported by another source.³⁸ These large absorption cross sections will allow single QDs to be visualized using significantly reduced illumination intensities, potentially reducing cellular photodamage, and allowing new, more compact excitation sources such as LEDs to be feasible alternatives to lasers and arc lamps. However, these large cross sections also make it particularly easy to inadvertently saturate QDs under what would normally be low illumination intensity.

Notably, the QDs measured here have a very low fluorescence saturation threshold compared with typical fluorophores: $k_x \sim 8 \times 10^6$ s⁻¹ was enough to saturate the T2-496 QDs while $k_x \sim 2 \times 10^8$ s⁻¹ was necessary for Alexa 488, which is typical of other organic dyes and green fluorescent proteins.^{39,40} The reduced fluorescence saturation threshold can be explained considering two factors: (1) greatly enhanced excitation cross section leads to higher excitation rates for the same excitation power, which leads to a higher flux of QDs into excited states, while slower decay rates from the excited states caused by the relatively slower components in multiexponential fluorescence decays of QDs,^{1,41} and (2) the large number of dark states with long off-times result in a significant bottleneck for those QDs to emit and return to the ground state. Thus, for single molecule

and biological imaging applications of QDs, it appears to be crucial to develop QDs that interconvert minimally with dark states. The reduced dark state occupancies in the Qdot565 and T2-496 dots and their relatively higher brightness seem to be promising properties that could potentially be further optimized for biological applications.

Effects from focal volume distortions upon fluorescence saturation are expected to increase the apparent diffusion time (decrease the apparent diffusion rate) because the effective observation volume becomes enlarged as more molecules from lower intensity regions can begin to contribute to the fluorescence signal comparably to those at the focus that are saturated. Thus, because of focal volume distortions and the very low expected photobleaching of QDs reported by other methods,^{2,12,13} it will likely be difficult to use FCS to estimate photobleaching quantum yields (Φ_B) of QDs, except in cases in which the bleaching yield is similar to that of organic dyes ($\Phi_B \sim 10^{-5}$). Also, quantitative fluorescence measurements, which rely on knowledge of the shape or size of the observation volume (such as confocal microscopy, 4Pi microscopy, and FCS), must consider distortions of the volume to be a possibility and either use appropriately low-intensity levels or correct for such distortions.

FCS as a Method To Measure Extinction Coefficients of Samples with Unknown Concentrations. We can measure the extinction coefficient of QDs without prior knowledge of the concentration; FCS gives the concentration and we use the absorbance then to calculate the extinction coefficient ϵ . Very large values for ϵ in QDs are observed at wavelengths relevant for biological imaging and these values are consistent with those previously reported in similar materials.^{5,42} We rely on the assumption that all absorbing QDs are bright (at least become bright on average during one diffusion time). It is straightforward to correct for a nonzero fraction of permanently dark absorbing QDs when such information is available.³³

Recent work by Yao et al.³³ shows that a significant fraction (~40–50%) of CdSe/ZnS core/shell QDs in aqueous solution are never radiant (permanently dark). If the QDs measured here also exhibit the same fraction of permanently dark (but still absorbing) particles, we will overestimate our extinction coefficients, which are based on the ratio of measured absorption divided by the concentration of bright QDs measured by FCS (which will be lower than the number of absorbing QDs if some are permanently dark). Thus our measured extinction coefficients ϵ_M may be corrected by a factor of $\epsilon_C \approx \epsilon_M(1 - F_{PD})$, where F_{PD} is the fraction of permanently dark (absorbing) QDs, and ϵ_C is the bright-fraction-corrected extinction coefficient.

Diffusion and Molecular Hydrodynamic Properties. The measured diffusion times of QDs in water correspond to hydrodynamic radii, which are significantly larger than the core diameter of a few (e.g., <5) nanometers observed by transmission electron microscopy (data not shown). For the T2-496 dots, the observed $r_H = 21.8 \pm 0.9$ nm is significantly larger than the value (~12.5 nm radius) reported by the manufacturer. Fitting the measured autocorrelation using the QD fitting function (eq 9) or with the standard fitting function allowing interconversions between one bright and two dark states (eq 1 with $m = 2$) resulted in similar values for the diffusion time within experimental uncertainty. The QD520s, which were coated with streptavidin, also showed similarly large hydrodynamic radii consistent with particle size much larger than the core plus cap. However, the QD560s, which were not coated with streptavidin, and the Qdot565s, which were coated with PEG, show significantly smaller r_H (7.6 ± 1.1 nm and $13.9 \pm$

0.8 nm, respectively), which are closer to the core size and may be advantageous in applications that require significant penetration through membranes and into cells. These differences in r_H may also reflect differences in interactions between the surface and the hydration shell in solution, not just physical size of core plus cap.

Even in pure water, it is not possible to eliminate aggregation of these QDs, which is expected to yield larger hydrodynamic radii, reduced brightness, and increased complexity of flicker. Attempts were made to concentrate and to break up aggregates, such as measurements of relatively dilute and concentrated aqueous solutions, and centrifugation (11000g for 10 min followed by measurement of the uppermost portion of the supernatant), which did not alter the measured diffusion time or eliminate the presence of occasional fluorescence bursts (which clearly show that some form of fluorescent aggregate was present). However, based on these bursts, a methodology was developed to quantify potential aggregation and used to detect strong evidence of aggregates in QD solutions in the presence of physiological concentrations of NaCl. On the basis of this methodology and the relatively low frequency of fluorescence bursts in pure water, (in the absence of significant concentrations of NaCl) the concentration of large aggregates can be estimated to be much less than 100 picomolar. Third, the absence of multiple diffusion components in the correlation at low intensity eliminates the possibility of large populations of highly fluorescent particles with disparate sizes. However, it is possible that the QDs observed in this study were dimerized or forming some other type of small, relatively monodisperse aggregates.

Use of QDs for Biological Imaging. Biological imaging of live cells is typically done in saline solutions (PBS) or media that contains significant concentrations of salt ions. Our result that aggregation of some QDs occurs in the presence of physiologically relevant concentrations of NaCl is therefore of considerable concern to developers of QDs for biological applications. We describe an FCS methodology for determining the size and extent of aggregates as well as the effect(s) of aggregation on fluorescence properties (including mobility and brightness).

If the only effect of aggregation is to reduce mobility without affecting brightness, this would be less problematic, but we also see evidence of quenching of dots as aggregation occurs. The fluorescence count rate dropped significantly upon addition of NaCl at concentrations as low as 10 mM into the solution containing QD520s. As the diffusion time increased, the number of monomers and/or small aggregates decreased, and the number of large fluorescent aggregates increased. Thus it appears that some form of precipitation-like process that sequesters monomers or smaller QD aggregates into large aggregates is occurring in the presence of NaCl. Because the number of QDs per aggregate is presumably increasing, we expected to see an overall brightness of an aggregate that would be approximately equal to the combined brightness of each QD in the aggregate, but this prediction was not realized in our observations. Although the overall brightness of an aggregate was greater than that of an individual QD, the brightness per QD in the aggregate was less than that of an individual QD. This shows that some or all of the QDs within the aggregates are not maintaining the brightness of a single QD. Thus, a significant problem with compatibility between the QD and the aqueous biological environment (or other comparable solution) needs to be overcome. On the other hand, the T2-496 and Qdot565 dots prepared by proprietary methods apparently did not suffer from

such aggregation. Clearly, a crucial step in the rise of QD technology depends on optimization of the coatings that solubilize the QDs in aqueous solution and can also be used to target QDs specifically to intracellular biological structures.

Reduced photobleaching of QDs is an advantageous property for many biological applications, especially where collection of single molecule information is desirable over long timescales. In ultraresolution methods such as FPALM,⁴³ PALM,⁴⁴ and STORM⁴⁵ the number of photons collected before photobleaching is a crucial parameter limiting localization-based resolution. QD that can be photoactivated, resist photobleaching, and show minimal intermittency would be ideal probes for localization-based ultraresolution imaging of biological samples.

Conclusions

We present a methodology for quantitatively determining certain photophysical parameters that are of interest to biological and single molecule users of QDs: count rate per molecule (brightness), luminescence flicker occupancy and interconversion rates, diffusion coefficient, hydrodynamic radius, extinction coefficient, and aggregation properties. We also present an improved FCS fitting function that successfully describes the autocorrelation of QDs in solution under all conditions tested. We find that among all QDs tested, the maximum QD brightness is higher when flicker rate is higher and when flicker occupancy is smaller. The enhanced brightness of the Qdot 565 and T2–496 QDs is apparently a result (in part) of faster interconversion rates between bright and dark states, which limit the time spent in dark states and therefore reduce the average occupancy of those dark states. The effect of synthesis methods on photophysical properties of QDs remains a question of crucial importance. Because the maximum brightness of a QD depends on limiting transitions of that QD into long-lived dark states, which are known in many cases to depend on trapping of displaced charge on QD surfaces, surface chemistry is clearly a crucial variable that must be further explored if QD properties are to be further optimized for biological imaging applications.

Acknowledgment. The authors would like to thank Karen Fancher, the Knowles Laboratory, the Mayer laboratory for the use of their Nanodrop systems, Lee Bickerstaff and Dr. Paul Millard for the use of their spectrofluorometer, Dr. Louise Brogan for providing samples of T2–496 QDs, Kelly Lundsten of Invitrogen for Qdot565 samples, Thomas Tripp for his machining services, Dr. Jim McClymer for the autocorrelator card, Dr. C. W. Smith for the microscope, and Drs. Paul Blank and Joshua Zimmerberg for the Argon-Ion laser. The work by J.A.R. was funded by an Integrative Graduate Education Research Traineeship (IGERT) fellowship sponsored by National Science Foundation Grant 0221625 awarded to the University of Maine (Orono, ME), The Jackson Laboratory (Bar Harbor, ME), and Maine Medical Center Research Institute (Scarborough, ME) in contribution to an interdisciplinary Ph.D. in Functional Genomics.

Nomenclature

α = multiplicative constant for QD dark state occupancy
 β = multiplicative constant for QD dark state interconversion rate
 γ = low-intensity slope of count rate per molecule versus excitation rate
 ϵ = molar absorbance
 ϕ = quantum yield for photoconversion or flicker
 Φ_B = photobleaching quantum yield

η = count rate per molecule
 η_{\max} = maximum count rate per molecule
 χ^2 = goodness of fit parameter
 λ = wavelength
 λ_x = excitation wavelength
 λ_d = detection wavelength
 ν = viscosity
 ρ = ratio of measured η to expected (extrapolated) η
 σ = absorption cross section
 τ = correlation time delay
 τ_D = diffusion time
 $\Omega(\vec{r})$ = detection volume profile
 ω = observation volume axial-to-lateral dimension ratio
 A = absorbance
 C = concentration
 D = measured diffusion coefficient
 F_{tot} = time-averaged fluorescence signal
 F_i = i^{th} dark state fraction
 F_{dark} = total fraction of dark molecules
 $G(\tau)$ = autocorrelation function
 $G_{\text{QD}}(\tau)$ = fitting function for QD autocorrelation
 $G_x(\tau)$ = standard analytical fitting function for autocorrelation
 I = excitation intensity
 $I_{\eta_{\max}}$ = intensity at which η is maximum
 I_{sat} = characteristic saturation intensity
 I_0 = peak intensity
 k_x = excitation rate
 k_B = Boltzmann's constant
 k_D = diffusion rate (the inverse of τ_D)
 k_i = i^{th} dark state interconversion rate (standard fitting function)
 k_f = flicker rate
 L = path length
 M = overall magnification
 m = number of independent transitions between bright and dark states
 n = refractive index
 N = number of molecules in the observation volume
 N_{bright} = number of bright molecules in the observation volume
 $N_{1\sigma}, N_{2\sigma}, N_{3\sigma}$ = number of fluorescence fluctuations within 1, 2, and 3 standard deviations of the mean, respectively
 NA = numerical aperture
 $O(\vec{r})$ = observation volume spatial profile (neglecting saturation effects)
 $O_s(\vec{r})$ = observation volume spatial profile (including saturation effects)
 QD = quantum dot
 \vec{r} = position (within the sample, measured relative to the focus)
 r_{BA} = objective back-aperture radius (real space)
 r_{beam} = $1/e^2$ beam radius (real space)
 r_d = confocal detector aperture radius (optical units)
 R_d = confocal detector aperture radius (real space)
 r_H = hydrodynamic radius
 r_0 = $1/e^2$ observation volume radius (real space)
 R_i = i^{th} dark state interconversion rate (QD fitting function)
 T = temperature
 V = volume (defined by $O(\vec{r})$)

$W(\bar{r})$ = observation volume (including saturation) normalized to 1 at max

References and Notes

- Hines, M. A.; Guyot-Sionnest, P. Synthesis and characterization of strongly luminescing ZnS-Capped CdSe nanocrystals. *J. Phys. Chem.* **1996**, *100*, 468–71.
- Chan, W. C.; Maxwell, D. J.; Gao, X.; Bailey, R. E.; Han, M.; Nie, S. Luminescent quantum dots for multiplexed biological detection and imaging. *Curr. Opin. Biotechnol.* **2002**, *13*, 40–6.
- Han, M.; Gao, X.; Su, J. Z.; Nie, S. Quantum-dot-tagged microbeads for multiplexed optical coding of biomolecules. *Nat. Biotechnol.* **2001**, *19*, 631–5.
- Mattoussi, H.; Mauro, J. M.; Goldman, E. R.; Anderson, G. P.; Sundar, V. C.; Mikulec, F. V.; Bawendi, M. G. Self-assembly of CdSe-ZnS quantum dot bioconjugates using an engineered recombinant protein. *J. Am. Chem. Soc.* **2000**, *122*, 12142–50.
- Dabbousi, B. O.; Rodriguez-Viejo, J.; Mikulec, F. V.; Heine, J. R.; Mattoussi, H.; Ober, R.; Jensen, K. F.; Bawendi, M. G. (CdSe)ZnS core-shell quantum dots: Synthesis and characterization of a size series of highly luminescent nanocrystallites. *J. Phys. Chem. B* **1997**, *101*, 9463–75.
- Klimov, V. I.; McBranch, D. W.; Leatherdale, C. A.; Bawendi, M. G. Electron and hole relaxation pathways in semiconductor quantum dots. *Phys. Rev. B* **1999**, *60*, 13740–49.
- Jaiswal, J. K.; Mattoussi, H.; Mauro, J. M.; Simon, S. M. Long-term multiple color imaging of live cells using quantum dot bioconjugates. *Nat. Biotechnol.* **2003**, *21*, 47–51.
- Kuno, M.; Fromm, D. P.; Hamann, H. F.; Gallagher, A.; Nesbitt, D. J. “On”/“off” fluorescence intermittency of single semiconductor quantum dots. *J. Chem. Phys.* **2001**, *115*, 1028–40.
- Gao, X.; Cui, Y.; Levenson, R. M.; Chung, L. W.; Nie, S. In vivo cancer targeting and imaging with semiconductor quantum dots. *Nat. Biotechnol.* **2004**, *22*, 969–76.
- Larson, D. R.; Zipfel, W. R.; Williams, R. M.; Clark, S. W.; Bruchez, M. P.; Wise, F. W.; Webb, W. W. Water-soluble quantum dots for multiphoton fluorescence imaging in vivo. *Science* **2003**, *300*, 1434–6.
- Chan, W. C.; Nie, S. Quantum dot bioconjugates for ultrasensitive nonisotopic detection. *Science* **1998**, *281*, 2016–8.
- Smith, A. M.; Gao, X.; Nie, S. Quantum dot nanocrystals for in vivo molecular and cellular imaging. *Photochem. Photobiol.* **2004**, *80*, 377–85.
- Gao, X.; Yang, L.; Petros, J. A.; Marshall, F. F.; Simons, J. W.; Nie, S. In vivo molecular and cellular imaging with quantum dots. *Curr. Opin. Biotechnol.* **2005**, *16*, 63–72.
- Jaiswal, J. K.; Simon, S. M. Potentials and pitfalls of fluorescent quantum dots for biological imaging. *Trends in Cell Biol.* **2004**, *14*, 497–504.
- Akerman, M. E.; Chan, W. C.; Laakkonen, P.; Bhatia, S. N.; Ruoslahti, E. Nanocrystal targeting in vivo. *Proc. Natl. Acad. Sci. U.S.A.* **2002**, *99*, 12617–21.
- Mitchell, G. P.; Mirkin, C. A.; Letsinger, R. L. Programmed assembly of DNA functionalized quantum dots. *Journal of the American Chemical Society* **1999**, *121*, 8122–23.
- Bruchez, M.; Moronne, M.; Gin, P.; Weiss, S.; Alivisatos, A. P. Semiconductor nanocrystals as fluorescent biological labels. *Science* **1998**, *281*, 2013–16.
- Wu, X. Y.; Liu, H. J.; Liu, J. Q.; Haley, K. N.; Treadway, J. A.; Larson, J. P.; Ge, N. F.; Peale, F.; Bruchez, M. P. Immunofluorescent labeling of cancer marker Her2 and other cellular targets with semiconductor quantum dots. *Nat. Biotechnol.* **2003**, *21*, 41–46.
- Nirmal, M.; Dabbousi, B. O.; Bawendi, M. G.; Macklin, J. J.; Trautman, J. K.; Harris, T. D.; Brus, L. E. Fluorescence intermittency in single cadmium selenide nanocrystals. *Nature* **1996**, *383*, 802–04.
- Kuno, M.; Fromm, D. P.; Hamann, H. F.; Gallagher, A.; Nesbitt, D. J. Nonexponential “blinking” kinetics of single CdSe quantum dots: A universal power law behavior. *J. Chem. Phys.* **2000**, *112*, 3117–20.
- Javier, A.; Strouse, G. F. Activated and intermittent photoluminescence in thin CdSe quantum dot films. *Chem. Phys. Lett.* **2004**, *391*, 60–63.
- Banin, U.; Bruchez, M.; Alivisatos, A. P.; Ha, T.; Weiss, S.; Chemla, D. S. Evidence for a thermal contribution to emission intermittency in single CdSe/CdS core/shell nanocrystals. *J. Chem. Phys.* **1999**, *110*, 1195–201.
- Doose, S.; Tsay, J. M.; Pinaud, F.; Weiss, S. Comparison of photophysical and colloidal properties of biocompatible semiconductor nanocrystals using fluorescence correlation spectroscopy. *Anal. Chem.* **2005**, *77*, 2235–42.
- Alivisatos, A. P. Semiconductor clusters, nanocrystals, and quantum dots. *Science* **1996**, *271*, 933–37.
- Hess, S. T.; Huang, S.; Heikal, A. A.; Webb, W. W. Biological and Chemical Applications of Fluorescence Correlation Spectroscopy: A Review. *Biochemistry* **2002**, *41*, 697–705.
- Peng, Z. A.; Peng, X. G. Formation of high-quality CdTe, CdSe, and CdS nanocrystals using CdO as precursor. *J. Am. Chem. Soc.* **2001**, *123*, 183–84.
- Albota, M.; Beljonne, D.; Bredas, J. L.; Ehrlich, J. E.; Fu, J. Y.; Heikal, A. A.; Hess, S. E.; Kogej, T.; Levin, M. D.; Marder, S. R.; McCord-Maughon, D.; Perry, J. W.; Rockel, H.; Rumi, M.; Subramaniam, C.; Webb, W. W.; Wu, X. L.; Xu, C. Design of organic molecules with large two-photon absorption cross sections. *Science* **1998**, *281*, 1653–56.
- Richards, B.; Wolf, E. Electromagnetic Diffraction in Optical Systems. 2. Structure of the Image Field in an Aplanatic System. *Proc. R. Soc. London, Ser. A* **1959**, *253*, 358–79.
- Butter, J. Y. P.; Hecht, B. Fast determination of saturation intensity and maximum emission rate by single-emitter imaging. *Opt. Express* **2006**, *14*, 9350–57.
- Hess, S. T.; Webb, W. W. Focal volume optics and experimental artifacts in confocal fluorescence correlation spectroscopy. *Biophys. J.* **2002**, *83*, 2300–17.
- Pawley, J. B. *Handbook of Biological Confocal Microscopy*, 2nd ed.; Plenum Press: New York, 1995.
- Heikal, A. A.; Hess, S. T.; Baird, G. S.; Tsien, R. Y.; Webb, W. W. Molecular spectroscopy and dynamics of intrinsically fluorescent proteins: Coral red (dsRed) and yellow (Citrine). *Proc. Natl. Acad. Sci. U.S.A.* **2000**, *97*, 11996–2001.
- Yao, J.; Larson, D. R.; Vishwasrao, H. D.; Zipfel, W. R.; Webb, W. W. Blinking and nonradiant dark fraction of water-soluble quantum dots in aqueous solution. *Proc. Natl. Acad. Sci. U.S.A.* **2005**, *102*, 14284–89.
- Abe, A.; Radin, N. S.; Shayman, J. A. Induction of glucosylceramide synthase by synthase inhibitors and ceramide. *Biochim. Biophys. Acta* **1996**, *1299*, 333–41.
- Gao, X.; Nie, S. Quantum dot-encoded mesoporous beads with high brightness and uniformity: rapid readout using flow cytometry. *Anal. Chem.* **2004**, *76*, 2406–10.
- Banin, U.; Cao, Y. W.; Katz, D.; Millo, O. Identification of atomic-like electronic states in indium arsenide nanocrystal quantum dots. *Nature* **1999**, *400*, 542–44.
- Murray, C. B.; Norris, D. J.; Bawendi, M. G. Synthesis and Characterization of Nearly Monodisperse Cde (E = S, Se, Te) Semiconductor Nanocrystallites. *J. Am. Chem. Soc.* **1993**, *115*, 8706–15.
- Schmelz, O.; Mews, A.; Basche, T.; Herrmann, A.; Mullen, K. Supramolecular complexes from CdSe nanocrystals and organic fluorophores. *Langmuir* **2001**, *17*, 2861–65.
- Hess, S. T.; Heikal, A. A.; Webb, W. W. Fluorescence Photoconversion Kinetics in Novel Green Fluorescent Protein pH Sensors. *J. Phys. Chem. B* **2004**, *108*, 10138–48.
- Widengren, J.; Rigler, R. Photobleaching investigations of dyes using fluorescence correlation spectroscopy (FCS). *Prog. Biophys. Mol. Biol.* **1996**, *65*, Ph109–Ph09.
- Dahan, M.; Laurence, T.; Pinaud, F.; Chemla, D. S.; Alivisatos, A. P.; Sauer, M.; Weiss, S. Time-gated biological imaging by use of colloidal quantum dots. *Opt. Letters* **2001**, *26*, 825–27.
- Vossmeier, T.; Katsikas, L.; Giersig, M.; Popovic, I. G.; Diesner, K.; Chemseddin, A.; Eychmuller, A.; Weller, H. Cds Nanoclusters - Synthesis, Characterization, Size-Dependent Oscillator Strength, Temperature Shift of the Excitonic-Transition Energy, and Reversible Absorbency Shift. *J. Phys. Chem.* **1994**, *98*, 7665–73.
- Hess, S. T.; Girirajan, T. P.; Mason, M. D. Ultra-High Resolution Imaging by Fluorescence Photoactivation Localization Microscopy (FPALM). *Biophys. J.* **2006**, *91*, 4258–72.
- Betzig, E.; Patterson, G. H.; Sougrat, R.; Lindwasser, O. W.; Olenych, S.; Bonifacino, J. S.; Davidson, M. W.; Lippincott-Schwartz, J.; Hess, H. F. Imaging intracellular fluorescent proteins at nanometer resolution. *Science* **2006**, *313*, 1642–5.
- Rust, M. J.; Bates, M.; Zhuang, X. Sub-diffraction-limit imaging by stochastic optical reconstruction microscopy (STORM). *Nat. Methods* **2006**, *3*, 793–6.
- Masuda, A.; Ushida, K.; Okamoto, T. New fluorescence correlation spectroscopy enabling direct observation of spatiotemporal dependence of diffusion constants as an evidence of anomalous transport in extracellular matrices. *Biophys. J.* **2005**, *88*, 3584–91.